

Article

# Chemical Structure and Magnetism of FeO<sub>x</sub>/Fe<sub>2</sub>O<sub>3</sub> Interface Studied by X-ray Absorption Spectroscopy

Ahmed Yousef Mohamed <sup>1,2</sup> , Won Goo Park <sup>3</sup> and Deok-Yong Cho <sup>1,\*</sup><sup>1</sup> IPIT & Department of Physics, Jeonbuk National University, Jeonju 54896, Korea; yousef@jbnu.ac.kr<sup>2</sup> Department of Physics, South Valley University, Qena 83523, Egypt<sup>3</sup> Center for Correlated Electron Systems, Institute for Basic Science, Seoul National University, Seoul 08826, Korea; pwg2005@snu.ac.kr

\* Correspondence: zax@jbnu.ac.kr; Tel.: +82-63-270-3444

Received: 30 July 2020; Accepted: 10 August 2020; Published: 14 August 2020



**Abstract:** The chemical and magnetic states of Fe/Fe<sub>2</sub>O<sub>3</sub> thin films prepared by e-beam evaporation were investigated by using element-specific techniques, X-ray absorption spectroscopy (XAS) and X-ray magnetic circular dichroism (XMCD). It was clearly shown that the Fe layers are oxidized to form an antiferromagnetic (AFM) FeO<sub>x<1</sub>, while the bottom oxide remained a weak ferromagnet (wFM) ( $\alpha+\gamma$ )-type Fe<sub>2</sub>O<sub>3</sub>. Dependences of the peak intensities and lineshapes on the Fe thickness and measurement geometry further demonstrate that FeO<sub>x<1</sub> layers reside mostly at the interface realizing an FM (Fe)/AFM (FeO<sub>x</sub>)/wFM (Fe<sub>2</sub>O<sub>3</sub>), whilst the spin directions lie in the sample plane for all the samples. The self-stabilized intermediate oxide can act as a physical barrier for spins to be injected into the wFM oxide, implying a substantial influence on tailoring the spin tunneling efficiency for spintronics application.

**Keywords:** FeO<sub>x</sub>; Fe<sub>2</sub>O<sub>3</sub>; X-ray absorption spectroscopy; X-ray magnetic circular dichroism; ferromagnet; antiferromagnet

## 1. Introduction

Fe–Fe<sub>2</sub>O<sub>3</sub> thin films constituting a ferromagnetic (FM)–antiferromagnetic (AFM) heterostructure have drawn attention in spintronics applications as they can serve as a key component in magnetic tunneling junctions (MTJs) or spin-valves [1–7]. The chemical and magnetic interactions at the Fe/Fe<sub>2</sub>O<sub>3</sub> interface have significance in determining the functionality, such as the tunneling magnetoresistance (TMR) ratio in the MTJs [1,4,8,9]. Thus, it is crucial to understand the interfacial magneto-chemistry at the atomic scale to tailor the spin transport property of the devices [9–13].

There are several methods to synthesize the Fe/Fe<sub>2</sub>O<sub>3</sub> thin films heterostructure: dip coating [14], ion sputtering deposition [3,15], e-beam evaporation [16,17], molecular beam epitaxy [8,18], etc. Among them, e-beam evaporation has advantages in that both Fe and Fe<sub>2</sub>O<sub>3</sub> layers can be deposited by one step without breaking the vacuum, and the oxidation of each layer can be controlled very efficiently simply by changing the oxygen partial pressure [19–21]. Particularly in the Fe/Fe<sub>2</sub>O<sub>3</sub> system, it was reported that including an FeO barrier between Fe and Fe<sub>2</sub>O<sub>3</sub> can enhance the TMR ratio [8,11]. Thus, the e-beam technique can be an optimal method to synthesize the intermediate oxide layers as well [16,17,22].

Meanwhile, the characterization of the magnetic interface using conventional magnetization measurement is challenging because of the small volume of the interfacial region. Besides, some paramagnetic signals from other sources, like substrate or electrodes, can interfere and hinder a straightforward interpretation of the data. Thus, it is desirable to discern the signals of Fe/Fe<sub>2</sub>O<sub>3</sub> from the others' by employing an element-specific probe for the chemical and magnetic properties investigation.

Therefore, in this work, we utilized X-ray absorption spectroscopy (XAS) which can capture the chemical and structural information of a specific element, i.e., Fe or O; The XAS at Fe L<sub>2,3</sub>-edge (K-edge) reflects the probability of Fe 2p → 3d (1s → p) intra-atomic electron excitations while the XAS at O K-edge does the probability of O 1s → 2p excitations. Figure 1 illustrates the geometry of the XAS measurement. Particularly in the case of soft XAS (at the Fe L- and O K-edges), the probing depth is very short (<5 nm) so that the signals mostly from the surface or interface layers can be captured. In addition, by conducting the XAS with circularly polarized X-rays (depicted by a spring-like curve in Figure 1) and examining the magnetic contrast of the films (called X-ray magnetic circular dichroism (XMCD)), the FM spin orders in the system can be scrutinized as well [23,24].

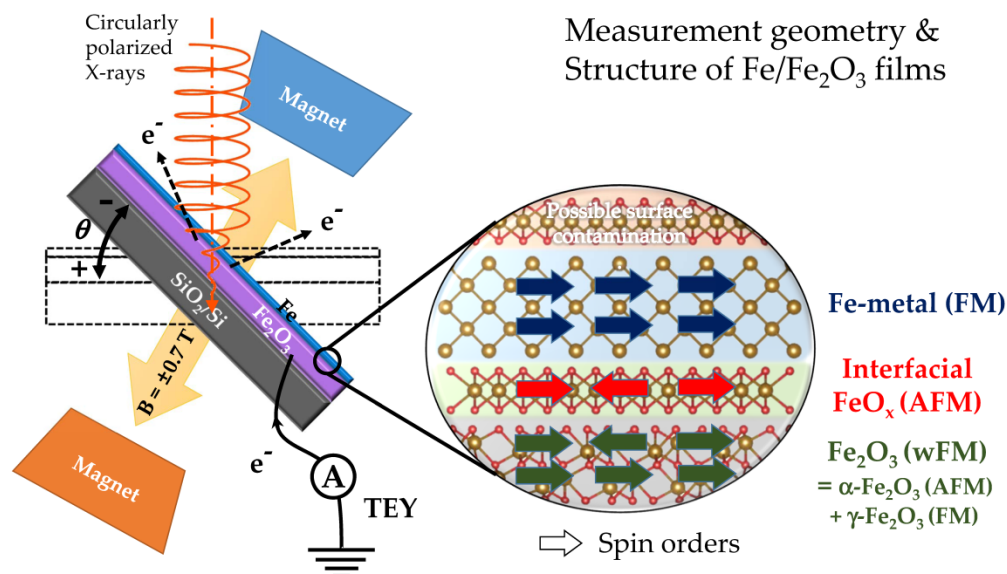


**Figure 1.** Schematics of the geometry of X-ray absorption spectroscopy (XAS) and X-ray magnetic circular dichroism (XMCD) measurements, and the atomic structures and magnetism of e-beam evaporated Fe/Fe<sub>2</sub>O<sub>3</sub> films according to the results of the analyses in this work.

The combined XAS and XMCD investigation not only shows the information on the interface chemistry and magnetism, but also reveals the local structures of the ultrathin Fe/Fe<sub>2</sub>O<sub>3</sub> thin films. The structural information enables a clear assessment of microstructures of the ultrathin oxide layers. The results of the analyses show that a substoichiometric FeO<sub>x</sub> (AFM) is formed spontaneously at the Fe/Fe<sub>2</sub>O<sub>3</sub> interface, while microstructures of Fe<sub>2</sub>O<sub>3</sub> turned out to be a mixture of a hematite (α-Fe<sub>2</sub>O<sub>3</sub>; AFM) [25] and a maghemite (γ-Fe<sub>2</sub>O<sub>3</sub>; FM) [26] structure, so that Fe<sub>2</sub>O<sub>3</sub> was, in fact, a weak FM (wFM), as is summarized in Figure 1.

## 2. Materials and Methods

Fe/Fe<sub>2</sub>O<sub>3</sub> thin films were prepared by e-beam evaporation using a commercial e-beam evaporator gun (EFM3, Omicron). The evaporation system's working pressure was < 1 × 10<sup>-7</sup> Torr for Fe deposition, while an oxygen gas was introduced with a partial pressure of 1 × 10<sup>-5</sup> Torr for the Fe<sub>2</sub>O<sub>3</sub> deposition. A tungsten wire of 0.2 mm thickness was used as a filament, and the voltage and the current of the e-beam emission to the fresh Fe rod 3 mm-apart, were maintained as 800 V and 11.4 mA, respectively. The evaporation rate was calibrated by a quartz crystal microbalance thickness monitor. The deposition rates of Fe and Fe<sub>2</sub>O<sub>3</sub> were fixed to 0.086 nm min<sup>-1</sup> and 0.176 nm min<sup>-1</sup>, respectively. First, a five nm-thick Fe<sub>2</sub>O<sub>3</sub> film was deposited on SiO<sub>2</sub>/Si substrate, then Fe film with 1 or 2 nm thickness was deposited additionally without breaking the vacuum to prevent unwanted oxidation or contamination at the Fe/Fe<sub>2</sub>O<sub>3</sub> interface. It was shown by Fe K-edge XAS that for a 20 nm-thick Fe film prepared under the same conditions that the film did not suffer oxidation during the deposition process itself.

However, the surface of the ultrathin Fe/Fe<sub>2</sub>O<sub>3</sub> specimen might be oxidized during the delivery to the synchrotron for the XAS measurement.

Soft XAS at Fe L<sub>2,3</sub>- and O K-edges were performed for the Fe/Fe<sub>2</sub>O<sub>3</sub> films with circularly polarized X-rays utilizing elliptically polarizing undulator at 2A beamline in Pohang Light Source (PLS). Absorption coefficients were collected with increasing photon energy in total electron yield (TEY) mode, in which the drain current (compensating the outgoing Auger electrons due to photoabsorption) was recorded. For the XMCD measurements, an external magnetic field (*B*) of 0.7 Tesla was applied with alternating directions, as shown in Figure 1, and the difference spectra of the two opposite *B* directions were obtained. The angle between the incident beam and magnetic field was set as 23°. In contrast, the samples were rotated by  $\theta = 0^\circ$  (beam normal),  $(-)$ 23° (magnet normal), or  $(+)$ 67° (magnet in-plane), where  $\theta$  is defined as in Figure 1, in order to examine the influences of the probing depth and the *B* direction. Hard XAS at Fe K-edge was conducted for thick Fe and Fe<sub>2</sub>O<sub>3</sub> films ( $\approx$ 20 nm) at 8C beamline in the PLS in fluorescence yield mode. The results of the characterizations are summarized in the right panel of Figure 1.

### 3. Results

Figure 2 shows the Fe L<sub>2,3</sub>-edge XAS and XMCD spectra of Fe (1 nm)/Fe<sub>2</sub>O<sub>3</sub> (5 nm) (abbreviated as '1/5 nm') and Fe (2 nm)/Fe<sub>2</sub>O<sub>3</sub> (5 nm) ('2/5 nm') films, as well as bare Fe<sub>2</sub>O<sub>3</sub> (5 nm) and Fe (5 nm) on SiO<sub>2</sub> for reference, which are taken at  $\theta = 0^\circ$ . Fe L<sub>3</sub> (L<sub>2</sub>)-edge XAS reflects the electron transition from the Fe 2p<sub>3/2</sub> (2p<sub>1/2</sub>) core level to the unoccupied Fe 3d orbital states, regardless of the spin ordering. Meanwhile, its evolution upon the change of the *B* direction from parallel to antiparallel to the incident X-rays, i.e., XMCD = [B//X-ray]-[B//-(X-ray)], reflects the magnetic contrast so that it can capture the signals from the FM-ordered Fe ions.

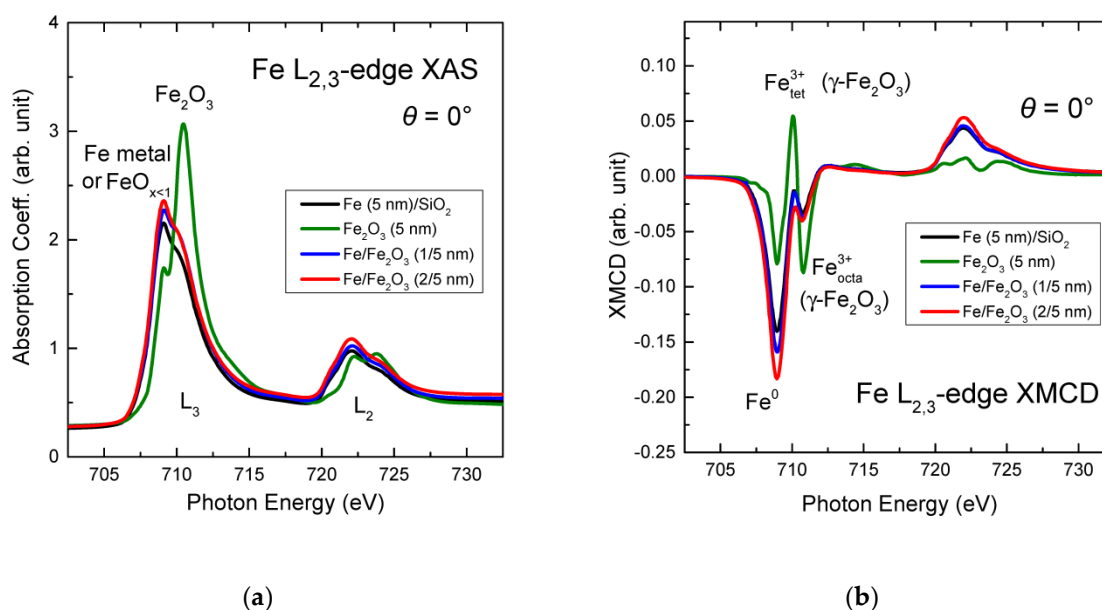


**Figure 2.** (a) Fe L<sub>2,3</sub>-edge XAS spectra and (b) Fe L<sub>2,3</sub>-edge XMCD spectra un-normalized. The spectra of Fe (1 or 2 nm)/Fe<sub>2</sub>O<sub>3</sub>, and Fe (5 nm)/SiO<sub>2</sub> samples exhibit the signature of Fe metal (or FeO<sub>x<1</sub>) as well as that of mixed ( $\alpha$ + $\gamma$ )-Fe<sub>2</sub>O<sub>3</sub>, suggesting a substantial degree of oxidation of the top Fe layers.

It is clearly shown in both XAS (Figure 2a) and XMCD (Figure 2b) spectra that the overall peak positions and lineshapes of the Fe/Fe<sub>2</sub>O<sub>3</sub> and Fe/SiO<sub>2</sub> samples are similar to each other, but they are very different from those of Fe<sub>2</sub>O<sub>3</sub>. In Figure 2a, the average energies of the main XAS peaks of the three samples at L<sub>3</sub>-edge (as well as at L<sub>2</sub>-edge) are lower than that of Fe<sub>2</sub>O<sub>3</sub>, suggesting an average Fe valence lower than 3+, such as in Fe metal or FeO [22,27]. In Figure 2b, only the signals from

the magnetic species, namely Fe metal (a dip from Fe<sup>0</sup>) and  $\gamma$ -Fe<sub>2</sub>O<sub>3</sub> (a peak from Fe<sup>3+</sup> in the tetrahedral site and a dip from Fe<sup>3+</sup> in the octahedral site in a maghemite structure), are observed [22,28]. Thus, it can be inferred that the Fe/Fe<sub>2</sub>O<sub>3</sub> and Fe/SiO<sub>2</sub> samples contain Fe metal, as was intended.

However, the XAS lineshapes of the three samples are different from a Fe metal [29], in that strong high energy shoulders exist at  $\approx$ 710 eV. It is not clear at this moment whether the shoulder peaks originate from Fe<sub>2</sub>O<sub>3</sub> at the bottom (or newly formed oxide in the case of Fe/SiO<sub>2</sub>) or represent an intrinsic property of the Fe layers themselves. It will be demonstrated in Figure 3 that FeO<sub>x<1</sub> exists at the Fe/Fe<sub>2</sub>O<sub>3</sub> interface, implying that the shoulder peaks might represent the electronic structure of the sub-stoichiometric FeO<sub>x</sub> [9,22,30]. Compared to the shoulder peak, the main peak at  $\approx$ 709 eV becomes slightly more enhanced as the Fe thickness increases, which is reasonable in that the metallic Fe would prevail in thicker Fe samples.

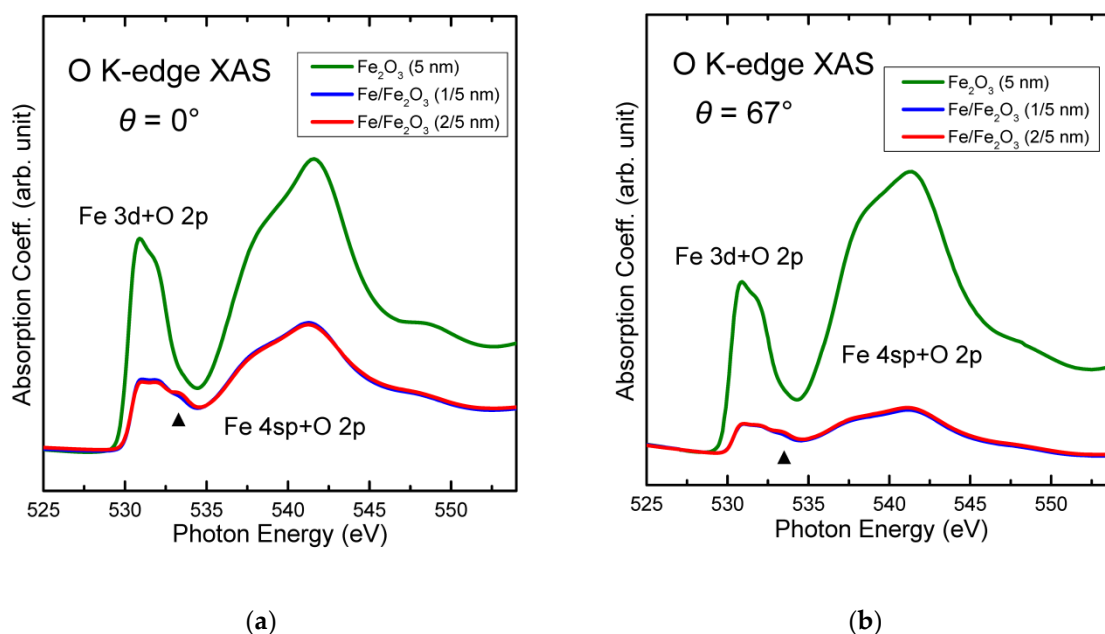


**Figure 3.** Un-normalized O K-edge XAS spectra taken (a) at  $\theta = 0^\circ$  (beam normal) and (b) at  $\theta = 66.5^\circ$ . Oxidized Fe formed FeO<sub>x<1</sub> mainly at the Fe/Fe<sub>2</sub>O<sub>3</sub> interface, which exhibits a fundamentally different electronic structure from  $(\alpha+\gamma)$ -Fe<sub>2</sub>O<sub>3</sub>.

Meanwhile, Fe<sub>2</sub>O<sub>3</sub> at the bottom might be in  $\alpha$  (AFM),  $\gamma$  (FM), or their mixed phase. The XAS spectra of  $\alpha$ - and  $\gamma$ -Fe<sub>2</sub>O<sub>3</sub> are generally very similar to each other, so it is difficult to discern the microstates using Fe L-edge XAS only [31]. Overall, XMCD signal of Fe<sub>2</sub>O<sub>3</sub> is much weaker than the XAS spectrum (<5%). The weak ferromagnetism implies that the AFM  $\alpha$  phase is rich in the Fe<sub>2</sub>O<sub>3</sub> films. The fraction of the  $\gamma$  phase (FM) over the  $\alpha$  phase, estimated from the intensity ratio of XMCD to XAS [28], was less than a half. Thus, in short, the Fe<sub>2</sub>O<sub>3</sub> at the bottom was weakly FM (wFM).

Figure 3 shows the O K-edge XAS spectra of 1/5 nm and 2/5 nm samples together with Fe<sub>2</sub>O<sub>3</sub> taken at (a)  $\theta = 0^\circ$  and (b)  $\theta = 67^\circ$ . O K-edge XAS reflects the electron transition from O 1s core level to O 2p unoccupied states that are hybridized with the orbitals of neighboring ions (here, Fe). The lower energy part (529–535 eV) represents the Fe 3d state hybridized with O 2p while the higher energy part (535–545 eV) does Fe 4sp state hybridized with O 2p. The lower energy part in the spectrum of Fe<sub>2</sub>O<sub>3</sub> exhibits the typical two-peak structure of Fe<sup>3+</sup> (d<sup>5</sup>, high spin), which can be attributed to t<sub>2g</sub>-e<sub>g</sub> split in the case of octahedral sites or e-t<sub>2</sub> split in the case of tetrahedral sites [16,32].

From comparison of Figure 3a with Figure 3b, it was noticed that the overall intensity of the Fe/Fe<sub>2</sub>O<sub>3</sub> films relative to that of Fe<sub>2</sub>O<sub>3</sub> decreased with increasing  $\theta$ . The angle dependence can be interpreted as a finite probing depth effect, in which the information from the deep layers cannot be collected as much as those from the surface, particularly when the incident X-rays are grazing to the sample plane [33]. Thus, the significant decrease in overall intensity of the Fe/Fe<sub>2</sub>O<sub>3</sub> samples in Figure 3b compared to Figure 3a (approximately by half) suggests that the O K-edge XAS signals are mostly from deep below the Fe layers. Since the O K-edge XAS signals manifest that there exist Fe-oxide, it can be told that certain Fe-oxide exists at the Fe/Fe<sub>2</sub>O<sub>3</sub> interface. Any surface oxidation effect is not consistent with the angle dependence.

It should be noted that there are additional Fe 3d states observed at  $\approx 534$  eV (highlighted by triangles) in the spectra of the two Fe/Fe<sub>2</sub>O<sub>3</sub> samples, indicative of the distinct chemistry of the interface oxide from Fe<sub>2</sub>O<sub>3</sub>. No such peaks were reported in stoichiometric oxides, including FeO, Fe<sub>3</sub>O<sub>4</sub>, or Fe<sub>2</sub>O<sub>3</sub> [21,34–38]. Therefore, the high energy states should be attributed to an additional energy level splitting due to a lower Fe-O coordination symmetry, which can be the case of sub-stoichiometric oxide, FeO<sub>x<1</sub> [9,32,39,40]. The formation of FeO<sub>x</sub> at the Fe/Fe<sub>2</sub>O<sub>3</sub> interface is plausible because Fe-oxides are generally more stable than Fe metal thermodynamically, and O would be easily supplied by Fe<sub>2</sub>O<sub>3</sub> to partially oxidize Fe near the interface region.

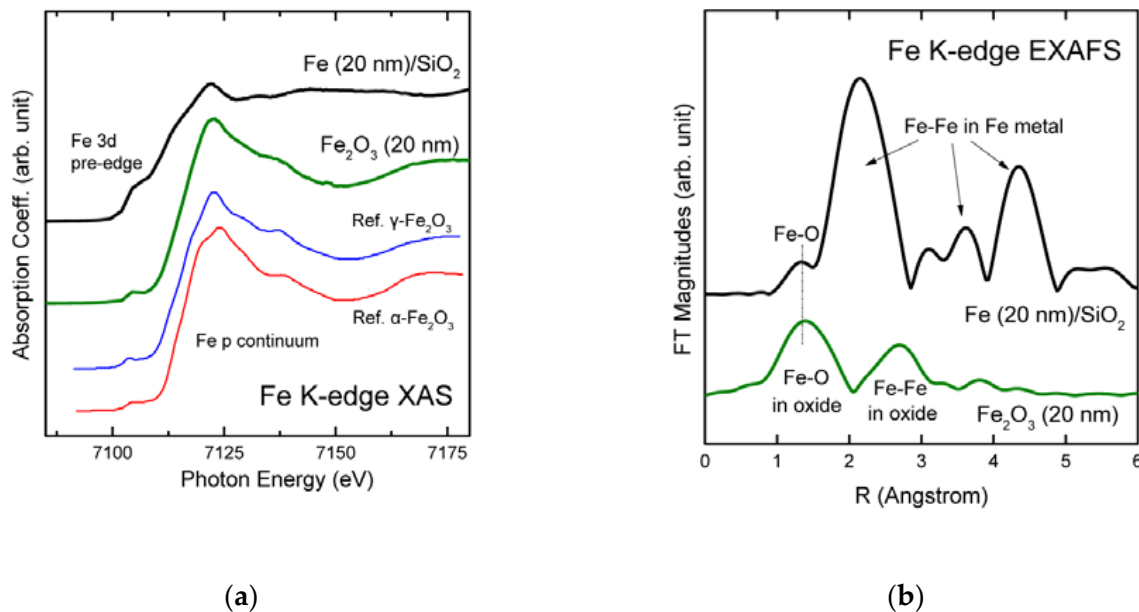
Figure 3 shows that the onsets of the lowest energy peaks in the spectra of Fe/Fe<sub>2</sub>O<sub>3</sub> samples are higher (by  $\approx 0.3$  eV) than that of Fe<sub>2</sub>O<sub>3</sub>. The higher onset energy suggests that the interfacial FeO<sub>x</sub> is an insulator. Besides, no noticeable peak or dip features, other than those for Fe or  $\gamma$ -Fe<sub>2</sub>O<sub>3</sub>, were observed in the Fe L-edge XMCD data (Figure 2b) in spite of nonzero nominal Fe valence in FeO<sub>x</sub> ( $+2x > 0$ ). This implies that the FeO<sub>x</sub> most plausibly has negligible FM order, i.e., should be almost an antiferromagnet [30,40,41]. Therefore, to summarize, an AFM FeO<sub>x</sub> is formed spontaneously between the FM Fe and wFM Fe<sub>2</sub>O<sub>3</sub> layers. This finding is illustrated in the right panel of Figure 1.

#### 4. Discussion

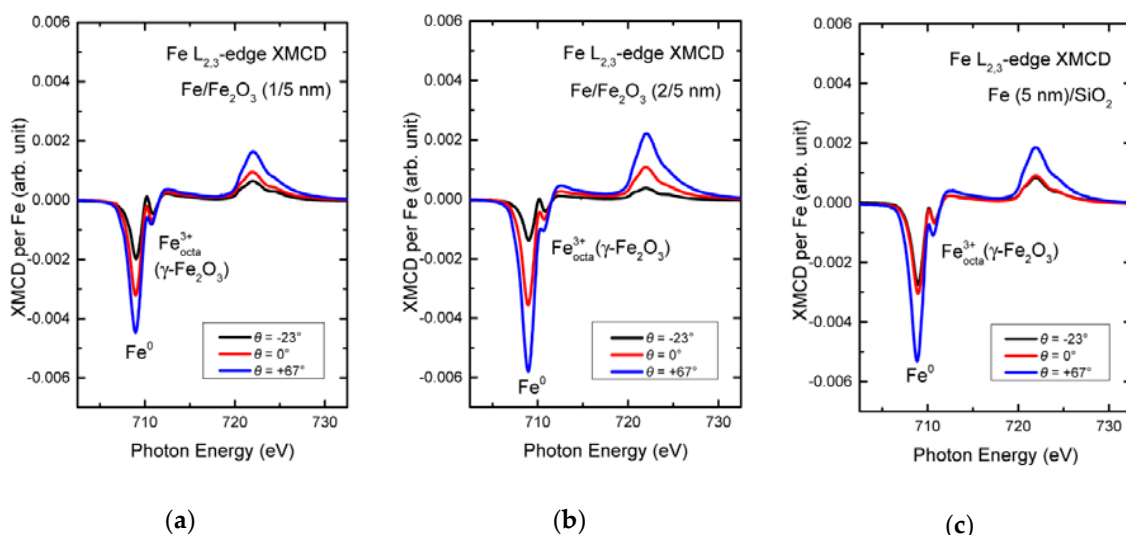
Regarding the origin of the interfacial FeO<sub>x</sub>, it needs to be clarified whether certain external factors in the growth process, e.g., remnant oxygen gas in the vacuum chamber, or uncleaned evaporation source, are responsible for the oxidation or not. Figure 4a shows the Fe K-edge XAS spectra of a thick Fe (20 nm) and Fe<sub>2</sub>O<sub>3</sub> (20 nm) films on SiO<sub>2</sub> prepared by the same growth condition, except for the increased thickness to enhance the signals of the hard XAS. Fe K-edge XAS reflects the transition from Fe 1s core level to Fe 3d (pre-edge region  $\approx 7110$  eV) or p-continuum ( $>7110$  eV), the fine structures of which result from the virtual scatterings of final state electrons with the neighboring atoms (here, O or Fe). Thus, the local structures near Fe can be analyzed by inspecting the lineshapes. The lineshape of the Fe sample was very similar to a reference Fe foil, while that of the Fe<sub>2</sub>O<sub>3</sub> sample was likely a combination of  $\alpha$ - and  $\gamma$ -Fe<sub>2</sub>O<sub>3</sub> [31,42–44]. The spectra of reference  $\alpha$ - and  $\gamma$ -Fe<sub>2</sub>O<sub>3</sub> taken from Sanson [45] are appended in the figure.

Figure 4b shows the Fourier-transformed (FT) extended X-ray absorption fine structures (EXAFS) magnitudes of the two samples. The FT was processed within a range of electron momentum  $k = 0\text{--}10 \text{ \AA}^{-1}$  on  $k^2$ -weighted EXAFS oscillations by using ATHENA [46]. The coordination shells can be identified according to the phase-uncorrected interatomic distance ( $R$ ) in  $\text{\AA}$ . For instance, the peak at  $R \approx 1.4 \text{ \AA}$  can be attributed to Fe–O bonds, while the peak at  $R \approx 2.1 \text{ \AA}$  can be to the shortest Fe–Fe bonds in a bcc Fe metal. It is clearly shown in the FT spectrum that Fe sample is most likely in the form of Fe metal (short Fe–Fe bonds), while a small portion of Fe-oxide (Fe–O bonds) can exist. The latter might reflect the oxidized Fe in Fe/SiO<sub>2</sub> film, which is already demonstrated in Figure 2. Nevertheless, Figure 4b conclusively shows that the composition of the Fe film was dominantly Fe metal. Hence, it can be concluded that the sample growth process was under control so that the Fe layers were not oxidized readily in the growth stage. Thus, the formation of FeO<sub>x</sub> should be regarded as a consequence of the interfacial interactions with Fe<sub>2</sub>O<sub>3</sub>.

Figure 5 shows the Fe  $L_{2,3}$ -edge XMCD spectra of (a,b) Fe/Fe<sub>2</sub>O<sub>3</sub> (1/5 nm and 2/5 nm) and (c) Fe (5 nm) taken at different  $\theta$ 's, after normalization by the XAS intensity in order to represent the magnetism per Fe atom. For all the samples, the intensities of the dips for Fe metal ( $\approx 709$  eV) and  $\gamma$ -Fe<sub>2</sub>O<sub>3</sub> ( $\approx 711$  eV) and the peaks for  $\gamma$ -Fe<sub>2</sub>O<sub>3</sub> ( $\approx 710$  eV) increase monotonically with increasing  $\theta$  from  $-23^\circ$  to  $+67^\circ$ .



**Figure 4.** (a) Fe K-edge near-edge XAS spectra and (b) the Fourier-transformed extended X-ray absorption fine structures (FT EXAFS) magnitudes of the thick Fe and Fe<sub>2</sub>O<sub>3</sub> films. The results show the films are indeed in their respective intended compositions, implying that the spontaneous Fe oxidations observed in the soft XAS data cannot be attributed to possible oxidation during the growth process.



**Figure 5.** Fe  $L_{2,3}$ -edge XMCD spectra normalized as to represent the signals per Fe atom at different  $\theta$ 's of (a) 1/5 nm, (b) 2/5 nm and (c) Fe (5 nm) samples. Overall XMCD intensity increases according to the incidence angle of the magnetic field (not the X-rays), indicating that the easy direction of the Fe and  $\gamma$ -Fe<sub>2</sub>O<sub>3</sub> spins lie in the sample planes for all the samples.

In principle, such an angle dependence can be ascribed either to the poling efficiency of the magnetic moments (both spin and angular moments) or to the spin sensitivity of the XMCD measurement itself [47]. The former concern is for cases where the coercivity (threshold value of  $B$  to align the spins)

is large and comparable with  $B$ , so that the size of the FM spins increases in accordance with  $B$ 's along the magnetic easy-axis of the specimen. In this case, the overall XMCD intensity would increase as a function of the angle between  $B$  and the sample's easy direction. On the other hand, the latter concern is that the circularly polarized X-rays can excite spins only parallel or antiparallel to the beam, so that the magnetic contrast observed in the XMCD appears inherently as a function of the angle between X-rays and the sample's easy-axis. In this case, the overall XMCD intensity will increase with the absolute value of  $\theta$ .

Since the XMCD intensities of the Fe/Fe<sub>2</sub>O<sub>3</sub> samples increased with increasing  $\theta$ , not the absolute value of  $\theta$ , it can be concluded that the ultrathin Fe/Fe<sub>2</sub>O<sub>3</sub> samples fall under the former case, i.e., the preferred orientations of the magnetic moments were in the sample planes for both the samples. For the case of the Fe (5 nm) sample, the two angle dependences would compete at  $\theta < 0^\circ$  to result in almost equal intensity of the  $\theta = -23^\circ$  and  $\theta = 0^\circ$  spectra.

Compared to 2/5 nm sample (Figure 5b), the  $\theta$  dependence is less abrupt in the 1/5 nm sample (Figure 5a). This reflects the weaker (more robust) tendency of the in-plane magnetization in 1/5 nm (2/5 nm) sample. As the thickness of the Fe layer decreases, the magnetic anisotropy tends to change from an in-plane magnetization to a perpendicular magnetization with a crossover thickness  $\approx 1$  nm [29,48]. Moreover, the presence of FeO<sub>x</sub> might reduce the magnetic volume of the heterostructure effectively, so as to expedite the tendency of the perpendicular magnetization. Therefore, it is reasonable that the magnetic anisotropy in 1/5 nm sample is less significant than 2/5 nm sample.

In conclusion, the XAS/XMCD study on ultrathin Fe/Fe<sub>2</sub>O<sub>3</sub> films provides unequivocal information on the chemistry, magnetism, and the local structures in the heterostructure system. The results of the detailed analyses indicate that the resultant composition is FM Fe/AFM FeO<sub>x</sub>/wFM ( $\alpha+\gamma$ )-Fe<sub>2</sub>O<sub>3</sub>, the spin orders of which are depicted with the arrows in the right panel of Figure 1. Although it is difficult to quantify the thickness of FeO<sub>x</sub> in 1/5 nm and 2/5 nm samples (due to small volume), the EXAFS data for thick Fe/SiO<sub>2</sub> implies that the Fe–O intensity is a few tens of percent of Fe<sub>2</sub>O<sub>3</sub>, suggesting FeO<sub>x</sub> can form up to a few-nm in thickness. The AFM FeO<sub>x</sub> layer can act as a physical barrier for spin transport from FM Fe to wFM Fe<sub>2</sub>O<sub>3</sub>, influencing the efficiency of the spin injection. Thereby, the e-beam growth of the FM/wFM (or AFM) heterostructure system can be a promising method for tailoring the spin tunneling properties for spintronics application by utilizing the parasitic FeO<sub>x</sub> formation.

**Author Contributions:** Conceptualization, D.-Y.C.; methodology, W.G.P.; formal analysis, A.Y.M.; writing, A.Y.M. and D.-Y.C. All authors have read and agreed to the published version of the manuscript.

**Funding:** This research was funded by National Research Foundation of Korea, grant number NRF-2018R1D1A1B07043427 and by Research Base Construction Fund Support Program in Jeonbuk National University in 2020.

**Conflicts of Interest:** The authors declare no conflict of interest. The funders had no role in the design of the study; in the collection, analyses, or interpretation of data; in the writing of the manuscript; or in the decision to publish the results.

## References

1. Khurshid, H.; Phan, M.-H.; Mukherjee, P.; Srikanth, H. Tuning exchange bias in Fe/ $\gamma$ -Fe<sub>2</sub>O<sub>3</sub> core-shell nanoparticles: Impacts of interface and surface spins. *Appl. Phys. Lett.* **2014**, *104*, 072407. [[CrossRef](#)]
2. Crisan, O.; von Haefen, K.; Ellis, A.; Binns, C. Structure and magnetic properties of Fe/Fe oxide clusters. *J. Nanopart. Res.* **2008**, *10*, 193–199. [[CrossRef](#)]
3. Kaur, M.; McCloy, J.S.; Qiang, Y. Exchange bias in core-shell iron-iron oxide nanoclusters. *J. Appl. Phys.* **2013**, *113*, 17D715. [[CrossRef](#)]
4. Signorini, L.; Pasquini, L.; Boscherini, F.; Bonetti, E.; Letard, I.; Brice-Profeta, S.; Sainctavit, P. Local magnetism in granular iron/iron oxide nanostructures by phase-and site-selective x-ray magnetic circular dichroism. *Phys. Rev. B* **2006**, *74*, 014426. [[CrossRef](#)]
5. Tang, D.; Wang, P.; Speriosu, V.; Le, S.; Kung, K. Spin-valve RAM cell. *IEEE Trans. Magn.* **1995**, *31*, 3206–3208. [[CrossRef](#)]

6. Parkin, S.S.P.; Roche, K.P.; Samant, M.G.; Rice, P.M.; Beyers, R.B.; Scheuerlein, R.E.; O'sullivan, E.J.; Brown, S.L.; Bucchigano, J.; Abraham, D.W.; et al. Exchange-biased magnetic tunnel junctions and application to nonvolatile magnetic random access memory. *J. Appl. Phys.* **1999**, *85*, 5828–5833. [[CrossRef](#)]
7. Quindeau, A.; Fina, I.; Marti, X.; Apachitei, G.; Ferrer, P.; Nicklin, C.; Pippel, E.; Hesse, D.; Alexe, M. Four-state ferroelectric spin-valve. *Sci. Rep.* **2015**, *5*, 9749. [[CrossRef](#)]
8. Wang, S.; Han, G.; Yu, G.; Jiang, Y.; Wang, C.; Kohn, A.; Ward, R. Evidence for FeO formation at the Fe/MgO interface in epitaxial TMR structure by X-ray photoelectron spectroscopy. *J. Magn. Magn. Mater.* **2007**, *310*, 1935–1936. [[CrossRef](#)]
9. Telesca, D.; Sinkovic, B.; Yang, S.-H.; Parkin, S. X-ray studies of interface Fe-oxide in annealed MgO based magnetic tunneling junctions. *J. Electron. Spectrosc. Relat. Phenom.* **2012**, *185*, 133–139. [[CrossRef](#)]
10. Lu, Y.; Claydon, J.S.; Ahmad, E.; Xu, Y.; Thompson, S.M.; Wilson, K.; van der Laan, G. XPS and XMCD study of Fe<sub>3</sub>O<sub>4</sub>/GaAs interface. *IEEE Trans. Magn.* **2005**, *41*, 2808–2810. [[CrossRef](#)]
11. Kim, D.; Lee, H.; Kim, G.; Koo, Y.; Jung, J.; Shin, H.; Kim, J.-Y.; Kang, J.-S. Interface electronic structures of BaTiO<sub>3</sub>@X nanoparticles (X =  $\gamma$ -Fe<sub>2</sub>O<sub>3</sub>, Fe<sub>3</sub>O<sub>4</sub>,  $\alpha$ -Fe<sub>2</sub>O<sub>3</sub>, and Fe) investigated by XAS and XMCD. *Phys. Rev. B* **2009**, *79*, 033402. [[CrossRef](#)]
12. Genuzio, F.; Mentes, T.; Freindl, K.; Spiridis, N.; Korecki, J.; Locatelli, A. Chemistry-dependent magnetic properties at the FeNi oxide–metal interface. *J. Mater. Chem. C* **2020**, *8*, 5777–5785. [[CrossRef](#)]
13. Tong, H.; Qian, C.; Miloslavsky, L.; Funada, S.; Shi, X.; Liu, F.; Dey, S. Studies on antiferromagnetic/ferromagnetic interfaces. *J. Magn. Magn. Mater.* **2000**, *209*, 56–60. [[CrossRef](#)]
14. Robbenolt, S.; Nicolenco, A.; Mercier Fernandez, P.; Auffret, S.; Baltz, V.; Pellicer, E.; Menéndez, E.; Sort, J. Electric field control of magnetism in iron oxide nanoporous thin films. *ACS Appl. Mater. Interfaces* **2019**, *11*, 37338–37346. [[CrossRef](#)] [[PubMed](#)]
15. Li, P.; Xia, C.; Zhu, Z.; Wen, Y.; Zhang, Q.; Alshareef, H.N.; Zhang, X.X. Ultrathin Epitaxial Ferromagnetic  $\gamma$ -Fe<sub>2</sub>O<sub>3</sub> Layer as High Efficiency Spin Filtering Materials for Spintronics Device Based on Semiconductors. *Adv. Funct. Mater.* **2016**, *26*, 5679–5689. [[CrossRef](#)]
16. Lu, Y.; Claydon, J.; Xu, Y.; Thompson, S.; Wilson, K.; Van der Laan, G. Epitaxial growth and magnetic properties of half-metallic Fe<sub>3</sub>O<sub>4</sub> on GaAs (100). *Phys. Rev. B* **2004**, *70*, 233304. [[CrossRef](#)]
17. Lu, Y.; Ahmad, E.; Xu, Y.; Thompson, S.M. Annealing-induced Fe oxide nanostructures on GaAs. *IEEE Trans. Magn.* **2005**, *41*, 3328–3330. [[CrossRef](#)]
18. Hassan, S.S.; Xu, Y.; Wu, J.; Thompson, S.M. Epitaxial Growth and Magnetic Properties of Half-Metallic Fe<sub>3</sub>O<sub>4</sub> on Si (100) Using MgO Buffer Layer. *IEEE Trans. Magn.* **2009**, *45*, 4357–4359. [[CrossRef](#)]
19. Paul, M.; Müller, A.; Ruff, A.; Schmid, B.; Berner, G.; Mertin, M.; Sing, M.; Claessen, R. Probing the interface of Fe<sub>3</sub>O<sub>4</sub>/GaAs thin films by hard x-ray photoelectron spectroscopy. *Phys. Rev. B* **2009**, *79*, 233101. [[CrossRef](#)]
20. Nozaki, T.; Kubota, H.; Fukushima, A.; Yuasa, S. Interface engineering using an Fe oxide insertion layer for growing a metastable bcc-Co on MgO (001). *Appl. Phys. Lett.* **2015**, *106*, 022405. [[CrossRef](#)]
21. Wong, P.J.; Zhang, W.; Wang, K.; van der Laan, G.; Xu, Y.; van der Wiel, W.G.; de Jong, M.P. Electronic and magnetic structure of C<sub>60</sub>/Fe<sub>3</sub>O<sub>4</sub> (001): A hybrid interface for organic spintronics. *J. Mater. Chem. C* **2013**, *1*, 1197–1202. [[CrossRef](#)]
22. Jiménez-Villacorta, F.; Prieto, C.; Huttel, Y.; Telling, N.; van der Laan, G. X-ray magnetic circular dichroism study of the blocking process in nanostructured iron-iron oxide core-shell systems. *Phys. Rev. B* **2011**, *84*, 172404. [[CrossRef](#)]
23. Stöhr, J.; Siegmann, H. *Magnetism: From Fundamentals to Nanoscale Dynamics*; Springer: Berlin/Heidelberg, Germany, 2006.
24. Miedema, P.S.; De Groot, F.M. The iron L edges: Fe 2p X-ray absorption and electron energy loss spectroscopy. *J. Electron. Spectrosc. Relat. Phenom.* **2013**, *187*, 32–48. [[CrossRef](#)]
25. Pauling, L.; Hendricks, S.B. The crystal structures of hematite and corundum. *J. Am. Chem. Soc.* **1925**, *47*, 781–790. [[CrossRef](#)]
26. Schulz, D.L.; McCarthy, G.J. X-ray powder data for an industrial maghemite ( $\gamma$ -Fe<sub>2</sub>O<sub>3</sub>). *Powder Diffr.* **1988**, *3*, 104–105. [[CrossRef](#)]
27. Lee, E.; Kim, D.; Hwang, J.; Lee, K.; Yoon, S.; Suh, B.; Hyun Kim, K.; Kim, J.-Y.; Jang, Z.; Kim, B.; et al. Size-dependent structural evolution of the biomineralized iron-core nanoparticles in ferritins. *Appl. Phys. Lett.* **2013**, *102*, 133703. [[CrossRef](#)]

28. Brice-Profeta, S.; Arrio, M.-A.; Tronc, E.; Menguy, N.; Letard, I.; dit Moulin, C.C.; Nogues, M.; Chanéac, C.; Jolivet, J.-P.; Saintavrit, P. Magnetic order in  $\gamma$ -Fe<sub>2</sub>O<sub>3</sub> nanoparticles: A XMCD study. *J. Magn. Magn. Mater.* **2005**, *288*, 354–365. [[CrossRef](#)]
29. Lee, J.-M.; Kim, J.-Y.; Yang, S.-U.; Park, B.-G.; Park, J.-H.; Oh, S.-J.; Kim, J.-S. Magnetism of pristine Fe films on GaAs (100). *Phys. Rev. B* **2007**, *76*, 052406. [[CrossRef](#)]
30. Radaelli, G.; Petti, D.; Plekhanov, E.; Fina, I.; Torelli, P.; Salles, B.; Cantoni, M.; Rinaldi, C.; Gutiérrez, D.; Panaccione, G.; et al. Electric control of magnetism at the Fe/BaTiO<sub>3</sub> interface. *Nat. Commun.* **2014**, *5*, 1–9. [[CrossRef](#)]
31. Cao, L.; Jiang, Z.-X.; Du, Y.-H.; Yin, X.-M.; Xi, S.-B.; Wen, W.; Roberts, A.P.; Wee, A.T.; Xiong, Y.-M.; Liu, Q.-S.; et al. Origin of magnetism in hydrothermally aged 2-line ferrihydrite suspensions. *Environ. Sci. Technol.* **2017**, *51*, 2643–2651. [[CrossRef](#)]
32. Pollak, M.; Gautier, M.; Thromat, N.; Gota, S.; Mackrodt, W.; Saunders, V. An in-situ study of the surface phase transitions of  $\alpha$ -Fe<sub>2</sub>O<sub>3</sub> by X-ray absorption spectroscopy at the oxygen K edge. *Nucl. Instrum. Methods Phys. Res. B* **1995**, *97*, 383–386. [[CrossRef](#)]
33. Trainor, T.P.; Templeton, A.S.; Eng, P.J. Structure and reactivity of environmental interfaces: Application of grazing angle X-ray spectroscopy and long-period X-ray standing waves. *J. Electron. Spectrosc. Relat. Phenom.* **2006**, *150*, 66–85. [[CrossRef](#)]
34. Bora, D.K.; Braun, A.; Erat, S.; Ariffin, A.K.; Löhnert, R.; Sivula, K.; Töpfer, J.; Grätzel, M.; Manzke, R.; Graule, T.; et al. Evolution of an oxygen near-edge X-ray absorption fine structure transition in the upper Hubbard band in  $\alpha$ -Fe<sub>2</sub>O<sub>3</sub> upon electrochemical oxidation. *J. Phys. Chem. C* **2011**, *115*, 5619–5625. [[CrossRef](#)]
35. Yang, C.K.; Chiou, J.W.; Tsai, H.M.; Pao, C.W.; Jan, J.C.; Ray, S.C.; Yeh, C.L.; Huang, K.C.; Hsueh, H.C.; Pong, W.F.; et al. Electronic structure and magnetic properties of Al-doped Fe<sub>3</sub>O<sub>4</sub> films studied by x-ray absorption and magnetic circular dichroism. *Appl. Phys. Lett.* **2005**, *86*, 062504. [[CrossRef](#)]
36. Chen, C.L.; Dong, C.L.; Rao, S.M.; Chern, G.; Chen, M.C.; Wu, M.K.; Chang, C.L. Investigation of the valence states of Fe and Co in Fe<sub>1-x</sub>Co<sub>x</sub>O<sub>y</sub> (0 < x < 1) thin films by x-ray absorption spectroscopy. *J. Condens. Matter Phys.* **2008**, *20*, 255236. [[CrossRef](#)]
37. Kumar, S.; Kumar, R.; Thakur, P.; Chae, K.H.; Sharma, S.K. Electronic structure studies of Mg<sub>0.95</sub>Mn<sub>0.05</sub>Fe<sub>2-2x</sub>Ti<sub>2x</sub>O<sub>4</sub> (0 ≤ x ≤ 0.8). *J. Magn. Magn. Mater.* **2008**, *320*, e121–e124. [[CrossRef](#)]
38. Shen, S.; Zhou, J.; Dong, C.-L.; Hu, Y.; Tseng, E.N.; Guo, P.; Guo, L.; Mao, S.S. Surface engineered doping of hematite nanorod arrays for improved photoelectrochemical water splitting. *Sci. Rep.* **2014**, *4*, 6627. [[CrossRef](#)]
39. Gautam, S.; Kane, S.N.; Park, B.G.; Kim, J.Y.; Varga, L.; Song, J.H.; Chae, K.H. XAS and XMCD studies of amorphous FeCo-based ribbons. *J. Non Cryst. Solids* **2011**, *357*, 2228–2231. [[CrossRef](#)]
40. Miyokawa, K.; Saito, S.; Katayama, T.; Saito, T.; Kamino, T.; Hanashima, K.; Suzuki, Y.; Mamiya, K.; Koide, T.; Yuasa, S. X-ray absorption and X-ray magnetic circular dichroism studies of a monatomic Fe (001) layer facing a single-crystalline MgO (001) tunnel barrier. *Jpn. J. Appl. Phys.* **2004**, *44*, L9–L11. [[CrossRef](#)]
41. Xu, M.; Li, M.; Khanal, P.; Habiboglu, A.; Insana, B.; Xiong, Y.; Peterson, T.; Myers, J.C.; Ortega, D.; Qu, H.; et al. Voltage-Controlled Antiferromagnetism in Magnetic Tunnel Junctions. *Phys. Rev. Lett.* **2020**, *124*, 187701. [[CrossRef](#)]
42. Pellegrain, E.; Hagelstein, M.; Doyle, S.; Moser, H.; Fuchs, J.; Vollath, D.; Schuppler, S.; James, M.; Saxena, S.; Niesen, L.; et al. Characterization of Nanocrystalline  $\gamma$ -Fe<sub>2</sub>O<sub>3</sub> with Synchrotron Radiation Techniques. *Phys. Status Solidi B* **1999**, *215*, 797–801. [[CrossRef](#)]
43. Olimov, K.; Falk, M.; Buse, K.; Woike, T.; Hormes, J.; Modrow, H. X-ray absorption near edge spectroscopy investigations of valency and lattice occupation site of Fe in highly iron-doped lithium niobate crystals. *J. Condens. Matter Phys.* **2006**, *18*, 5135. [[CrossRef](#)]
44. Bora, D.K.; Braun, A.; Erat, S.; Safonova, O.; Graule, T.; Constable, E.C. Evolution of structural properties of iron oxide nano particles during temperature treatment from 250 °C–900 °C: X-ray diffraction and Fe K-shell pre-edge X-ray absorption study. *Curr. Appl. Phys.* **2012**, *12*, 817–825. [[CrossRef](#)]
45. Sanson, A. Comment on ‘On the discrimination between magnetite and maghemite by XANES measurements in fluorescence mode’. *Meas. Sci. Technol.* **2013**, *24*, 118001. [[CrossRef](#)]
46. Ravel, B.; Newville, M. ATHENA, ARTEMIS, HEPHAESTUS: Data analysis for X-ray absorption spectroscopy using IFEFFIT. *J. Synchrotron Radiat.* **2005**, *12*, 537–541. [[CrossRef](#)]

47. Stöhr, J. Exploring the microscopic origin of magnetic anisotropies with X-ray magnetic circular dichroism (XMCD) spectroscopy. *J. Magn. Magn. Mater.* **1999**, *200*, 470–497. [[CrossRef](#)]
48. Kim, W.; Choi, J.H.; Nahm, T.U.; Song, S.H.; Oh, S.J. Magnetic properties of ultrathin Fe films on Pt (111) and Pd (111): A surface magneto-optic Kerr effect study. *J. Korean Phys. Soc.* **2004**, *44*, 722–725.



© 2020 by the authors. Licensee MDPI, Basel, Switzerland. This article is an open access article distributed under the terms and conditions of the Creative Commons Attribution (CC BY) license (<http://creativecommons.org/licenses/by/4.0/>).